



# Mechanical properties and permeability evolution in gas-bearing coal–rock combination body under triaxial conditions

Kai Wang<sup>1,2</sup> · Feng Du<sup>1,2</sup> · Xiang Zhang<sup>2</sup> · Liang Wang<sup>1,2</sup> · Chengpeng Xin<sup>2,3</sup>

Received: 28 June 2017 / Accepted: 27 November 2017 / Published online: 16 December 2017  
© Springer-Verlag GmbH Germany, part of Springer Nature 2017

## Abstract

With the development of deep mining in recent years, coal and gas compound dynamic disasters become increasingly serious. In this study, uniaxial and triaxial compression tests were conducted on gas-bearing coals, coal–sandstone combined bodies and coal–mudstone combined bodies and the permeabilities in the triaxial tests were measured simultaneously. The mechanical behavior and seepage characteristics of coals and coal–rock combination bodies under triaxial conditions were compared in details. The results show that the peak strength among three samples is: coal–sandstone combined body > coal–mudstone combined body > coal. If other conditions were held constant, the strength and the elastic modulus of all specimens show that tendency increases with the increment of the confining pressure or with the decrease in the gas pressure. The strength characteristics of all three specimens met the Mohr–Coulomb criterion, and the residual strength has an increasing trend with the increase in confining pressure. The permeability evolutions of gas-bearing coals and coal–rock combination bodies which are determined by the crack propagation in the coals and rocks are not exactly the same. This preliminary study is intended to deepen our understandings of the mechanisms of coal–gas compound dynamic disasters and provide theoretical bases for their predictions.

**Keywords** Deep mining · Coal–gas compound dynamic disasters · Coal–rock combination body · Triaxial compression · Permeability

## Abbreviations

C–M Coal–mudstone  
C–S Coal–sandstone

## Introduction

Coal and gas outburst and rockburst (here using “rockburst” to avoid showing a preference for the USA of coal bump or Australia of coalburst) are the two most typical coal and rock dynamic disasters during underground mining (Lama and Bodziony 1998; Li et al. 2015; Zhu et al. 2016a, b). In shallow mining, these two kinds of dynamic disasters usually occur independently. In recent years, coal and rock dynamic disasters become more serious with the gradual increase in mining intensity and depth. Meanwhile, the form of disaster is evolved from a single typical dynamic disaster (coal–gas outburst or rockburst) to a compound form. And these two kinds of dynamic disasters coexist, interrelate, combine and transform reciprocally, as a result some coal and rock dynamic disasters have both characteristics of coal–gas outbursts and of rockbursts, to which are commonly referred to as coal–gas compound dynamic disasters in Chinese coal industry (Pan 2016; Sun and Li 2011). For instance, on March 14, 1945, at the Kenilworth coal mine in America, a rockburst occurred with unusual gas emission and a large amount of thick coal dust. Then, the mine

✉ Kai Wang  
kaiwang@cumtb.edu.cn

✉ Feng Du  
fengducumtb@126.com

<sup>1</sup> Beijing Key Laboratory for Precise Mining of Intergrown Energy and Resources, China University of Mining and Technology (Beijing), Beijing 100083, China

<sup>2</sup> Faculty of Resources and Safety Engineering, China University of Mining and Technology (Beijing), Beijing 100083, China

<sup>3</sup> School of Mining Engineering, Guizhou University of Engineering Science, Bijie 551700, China

exploded, severely burning 12 miners. Seven of the injured died eventually. On April 15, 1981, a gas outburst-induced rockburst disaster occurred at the Dutch Creek No. 1 Mine in Colorado, resulting in fifteen miners killed and three injured (Iannacchione and Zelanko 1995). In China, a rockburst-induced gas outburst (unusual gas emission) disaster occurred at the Sunjiawan coal mine in Fuxin on February 14, 2005, which killed 214 miners (Li et al. 2007). Another coal–gas outburst-induced rockburst disaster occurred in Yangou coal mine in Jiangxi Province on November 8, 2012 (Chen 2013).

Coal–gas compound dynamic disasters are essentially the failure of the whole coal–rock combination system under the combined actions of strong engineering disturbance, certain ground stress and gas pressure. On the one hand, under the actual mining disturbance, the instability caused by breaking or slipping of the hard roof (floor) will cause a large amount of elastic energy to be suddenly released, leading to the occurrence of rockburst. Meanwhile, the coal and gas outburst may be induced by the occurrence of rockburst, which generally presents the compound characteristics. On the contrary, the released energy of the coal and gas outburst induced by the mining disturbance may result in the instability of coal–rock combination system. Therefore, rockburst is induced by outbursts. When the coal or rock and stored gas in deformation zones release energy at the same time, the outburst and rockburst coupling dynamic disaster usually occurs (Pan 2016). On the other hand, the occurrences of the above three forms of coal–gas compound dynamic disasters are closely related to the damage, deformation, fractures and seepage behavior of coal and rock combination structures. Therefore, the study of the failure characteristics and gas flow behavior of coal–rock combination body under different gas pressure is of great significance to predict and control coal–gas compound dynamic disasters.

Currently, many scholars made a large number of research achievements on the deformation and strength behavior of coal–rock combination bodies. Petukhov and Linkov (1979) analyzed the stability of coal–rock combination system while studying the post-peak damage characteristics. Many researchers analyzed the influence of confining pressure (Zuo et al. 2016), loading rate and path (Huang and Liu 2013; Zuo et al. 2011a; Zhu et al. 2016a, b), combination modes (Zhang et al. 2012) and combination-inclined angles (Guo et al. 2011) on the mechanical properties of coal–rock combination bodies. Zuo et al. (2011b), Wang et al. (2013), Dou et al. (2005) and Zhao et al. (2008) discussed the characteristics of acoustic emission, electromagnetic radiation and infrared in the failure process of coal–rock combination bodies. Considering different interface effects, Zhao et al. (2014, 2015, 2016) investigated the failure characteristics and compression–shear strength criterion of coal–rock combination model. Liu et al. (2014) studied the effect of rock

strength on failure mode and mechanical behavior of composite bodies and drew the conclusion that the peak strength of the combination bodies decreases with the rock strength increasing. Besides, in terms of the numerical simulation, some scholars (Bao et al. 2013; Chen et al. 1997; Deng et al. 2012; Li et al. 2012; Lin et al. 1999; Liu et al. 2004a, b; Wang 2006; Zhao et al. 2013a, b; Tan et al. 2016) simulated the failure process of coal–rock combination system using process analysis (RFPA) and FLAC3D. Meanwhile, the unstable precursors, resilience, strain localization and size effect were discussed. Moreover, there have been many studies concerning the permeability evolution of gas in coals (Clarkson and Bustin 1999; Palmer and Mansoori 1996; Siriwardane et al. 2009; Wang et al. 2017a; Xie et al. 2015) and the mechanical behavior of coals (George and Barakat 2001; Masoudian et al. 2014; Perera et al. 2013; Ranjith et al. 2010; Viete and Ranjith 2007; Yang et al. 2015). However, most of above studies have ignored the influence of gas pressure on the deformation and failure characteristics of coal–rock combination body. And the gas seepage law in combination body has seldom been studied. In present work, the triaxial compression tests were carried out for Xinjing gas-bearing coals, coal–sandstone combined bodies and coal–mudstone combined bodies. And the permeability in the triaxial tests was measured simultaneously. The failure mechanism and mechanical behavior of coals and coal–rock combination bodies under different gas pressures were compared in detail under triaxial condition. As a result of these experiments, theoretical references are provided for mechanism study of coal–gas compound dynamic disasters and their predictions.

## Experimental methods

### Samples preparation

The coal and rock samples were taken from the 15# working face and its immediate roof of the Xinjing coal mine in Yangquan City, Shan Xi Province, China. The geographical location of the coal mine is shown in Fig. 1. And the local stratigraphic map of coal seam 15# in Xinjing coal mine is depicted in Fig. 2. The sample coal seam was buried 780 m under ground and is anthracite. The coal seam in the working face is a stable medium-thickness seam, and the average coal thickness is 6.51 m. The component of the immediate roof is mainly mudstone whose thickness is 0–10.22 m. Besides, some immediate roof is thinned locally and replaced by sandstone.

The tested specimens are drilled from a large-scale coal or rock sample. For single coal, sandstone and mudstone specimens, the samples were drilled in the laboratory into cylindrical shape samples with a diameter of 50 mm and

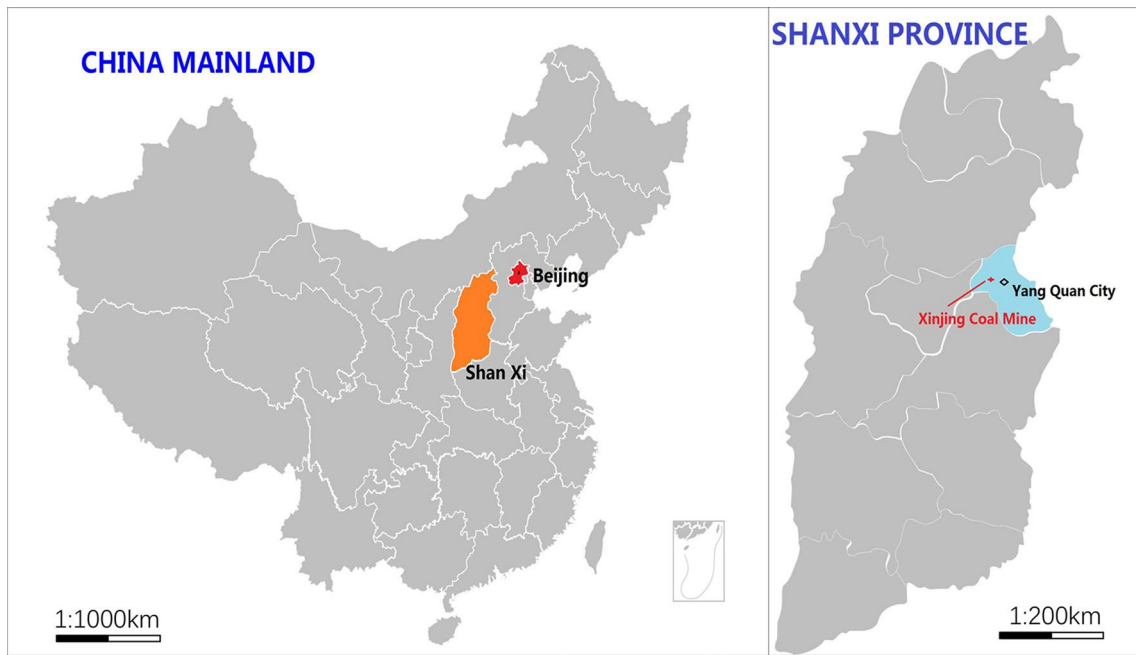


Fig. 1 Geographical location of the Xinjing coal mine

Fig. 2 Local stratigraphic map of coal seam 15# in Xinjing coal mine

Rock thickness (m)	Depth (m)	Columnar	Lithology
2.10	752.77		Fine-grained sandstone
3.10	755.87		Limestone
4.11	759.98		Mudstone
4.28	764.26		Fine-grained sandstone
1.00	765.26		Mudstone
1.60	766.86		Fine-grained sandstone
4.14	771.00		Mudstone
3.40	774.40		Limestone
8.25	782.65		Mudstone
6.51	789.16		Coal seam 15#
16.60	805.76		Sandy mudstone

height of 100 mm. For coal–rock combination specimen, in order to basically mimic the real coal–rock seam on site, the height ratio of the immediate roof and coal is 1:1. Therefore, the immediate roof (sandstone/mudstone) and coal are processed into  $\Phi 50$  mm  $\times$  50 mm, which are combined into a standard composed body of  $\Phi 50$  mm  $\times$  100 mm. In order to reduce the influence of the cracks on the experimental results of coal and rock specimens, the wave velocities of specimens were measured firstly. Then, the specimens with similar wave velocities are chosen to carry out the tests. It should be noted that in order to reduce the factors influencing the failure of the combination specimens, the coal part and rock part contact each other directly without any superglue in interface (Zuo et al. 2016). And the side face of the combination bodies was fixed with scotch tape. The finished samples are shown in Fig. 3.

### Testing system

All uniaxial and triaxial tests were carried out using the RLW-500G triaxial creep–seepage–adsorption and desorption experimental system at Henan Polytechnic University. The schematic diagram of the test system is shown in Fig. 4. The triaxial loading machine has a maximum axial load capacity of 500 kN, a maximum confining load capacity of 50 MPa, a uniaxial lateral extensometer range of 0–7 mm and an axial stroke of 0–14 mm. The accuracy of each sensor is  $\pm 0.5\%$  around the range. In this work, for coal–rock combined body, the following methods are used to measure the strain: the stress is the whole stress of the coal–rock combined body, and the axial strain is the strain of rock part and of coal part. Because the circumferential deformation of coal is larger than that of rock, the circumferential strain gauge is placed on the coal body.



**Fig. 3** Map of coal, coal–sandstone/mudstone combined body

## Testing program and procedures

### Uniaxial compression tests

Uniaxial compression tests are important to study the basic mechanical properties of coal and rock. In order to understand the basic mechanical behavior of single coal, rock and combination bodies and provide the basis for triaxial tests, conventional uniaxial compressive tests were carried out on single coals, sandstones, mudstones, coal–sandstone combined bodies and coal–mudstone combined bodies. The mechanical properties and failure behavior of five samples under uniaxial conditions were compared in details.

### Triaxial stress–permeability tests

Conventional triaxial stress–permeability tests were carried out on coals, coal–sandstone combined bodies and coal–mudstone combined bodies. Due to the relevant provisions about methane gas in the laboratory,  $\text{CH}_4$  is forbidden to use to ensure the safety of laboratory tests. Meanwhile, in this work, because both  $\text{CO}_2$  and  $\text{CH}_4$  are adsorptive gases and coal seam gases, and the adsorption of  $\text{CO}_2$  and  $\text{CH}_4$  in coals show many similar properties (Busch and Gensterblum 2011; Day et al. 2012; Gensterblum et al. 2013; Wang et al. 2017b), the gas selected in these tests was carbon dioxide of 99.99% purity, which replaced coal seam gas approximately. All of the gases mentioned below refer to the carbon dioxide above. The specific procedures for triaxial stress–permeability tests are as follows:

- (1) Sample installation. Firstly, silicone rubber was applied to both sides of the coal sample. Meanwhile, a certain length of heat-shrinkable tube was attached to the sample and a hot air gun was used to heat it evenly in order to make the coal sample completely jointed with the heat-shrinkable tube. Then, the axial and radial deformation sensors were installed on the specimen. Next, the sample was placed into the pressure chamber. Finally, upstream inlet line and downstream outlet line were connected, and the shroud of triaxial cell was covered.
- (2) Vacuum pumping. The axial pressure head was manipulated to touch the specimen, and the air in the pressure chamber was emptied. Then, a certain axial stress and confining stress of 4 MPa (hydrostatic pressure) were set on the sample. The system was vacuumed for 8 h to extract the impure gases. Meanwhile, the potential leakage within the entire system was investigated to ensure the reliability of experimental data.
- (3) Gas adsorption equilibrium. The temperature of the load module and flow module was set as constant by temperature control system. The high-pressure gas

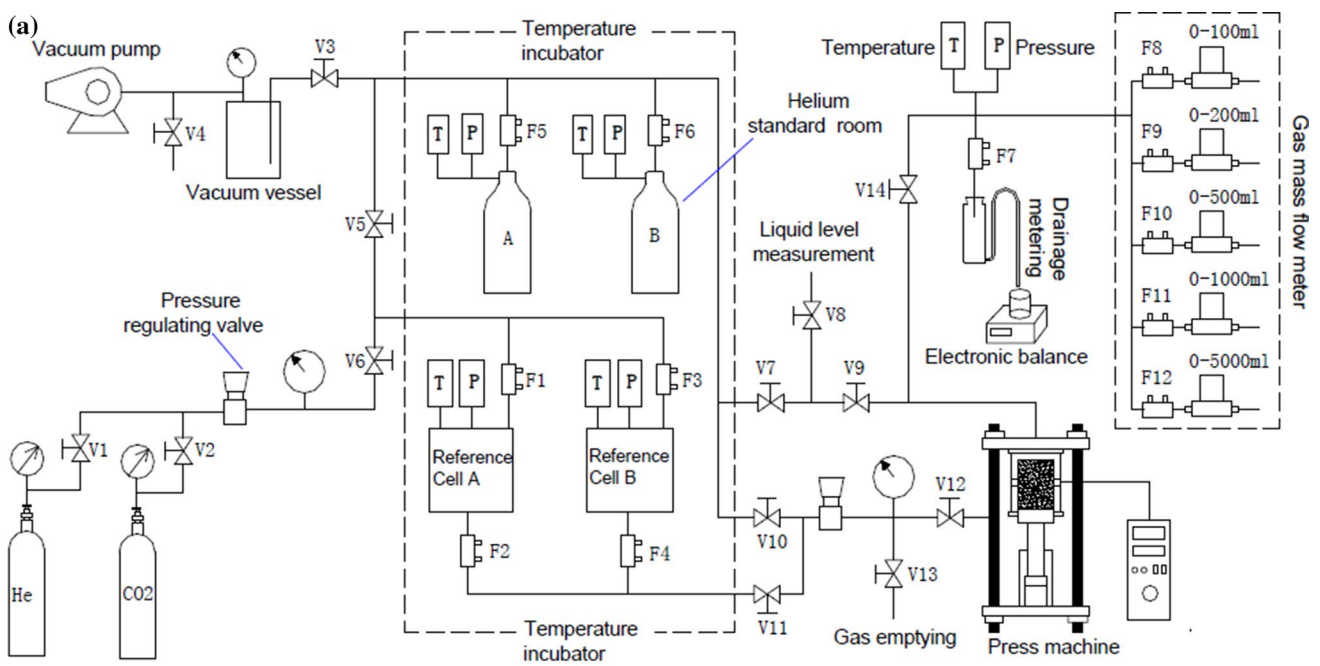


**Fig. 4** Triaxial creep–seepage experimental system **a** Schematic diagram of testing system. **b** The map of testing system

- ( $p = 1.5, 2, 2.5$  MPa) was injected into the core holder so that gas was fully adsorbed into the sample. The adsorption time keeps at least 60 h. When the axial strain is almost stable, the adsorption equilibrium state is considered to be reached.
- (4) Testing process. The mechanical loading tests were carried out with the gas outlet opening and loading device turning on. Meanwhile, the real-time permeability of the sample was measured until the test is finished.
  - (5) The tests were repeated by changing the confining pressure to 7 MPa and 10 MPa, respectively, and the gas pressure was fixed at 2 MPa.

- (6) The procedures (1)–(5) were repeated by replacing the coal sample with coal–rock combined bodies. Once a test failed, the re-experiment was made up immediately.

## Results

### Uniaxial mechanical properties of coal and coal–rock combined body

The stress–strain curves and the basic physical and mechanical parameters of coal and coal–rock combined bodies under

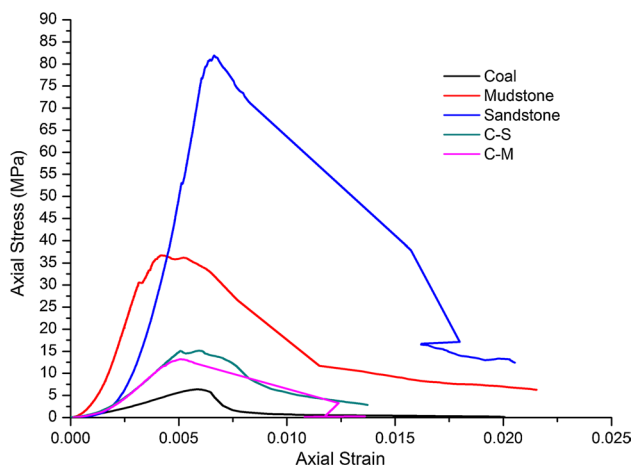


**Fig. 5** The stress–strain curves of five specimens under uniaxial conditions (“C–S” represents coal–sandstone combined body, “C–M” represents coal–mudstone combined body)

**Table 1** The basic physical and mechanical parameters of five specimens under uniaxial conditions

Sample	Peak strength $\sigma_1$ (MPa)	Wave velocity $V$ ( $\text{m s}^{-1}$ )	Elastic modulus ( $E$ /GPa)
Coal	6.38	1570	1.305
Mudstone	36.21	3752	15.238
Sandstone	81.9	3156	26.536
C–M	13.17	2656	3.923
C–S	15.13	2384	3.986

uniaxial conditions are shown in Fig. 5 and Table 1. It can be seen from Fig. 5 that the stress–strain curves of five specimens have undergone five stages under uniaxial condition: fracture compression, elastic deformation, plastic deformation, strain softening and plastic flow. After the peak stress, the stress shows obvious “stress drop” phenomenon, and

the dropping velocities of different specimens are different: sandstone > mudstone > coal–sandstone combined body > coal–mudstone combined body > coal. The tests results show that the uniaxial compressive strengths of five specimens are 81.90, 36.21, 15.13, 13.17 and 6.38 MPa, respectively. And the elastic moduli of five specimens are 26.536, 15.238, 3.986, 3.923 and 1.305 GPa, respectively. Therefore, the strength of the coal–rock combination body falls in between the single rock and coal. Moreover, the strength of coal–sandstone combined body is slightly larger than that of coal–mudstone combined body, indicating that the greater the rock strength in the coal–rock composite is, the greater the strength of the coal–rock combined body when the coal strength is constant. There are two main reasons for that. On the one hand, the rock body has high bearing capacity, which has a significant constraint effect on the deformation of coal body in the failure process of combined body. This constraint effect leads to the enhancement of its overall bearing capacity, and the constraint effect is more obvious with the increase in the rock strength. On the other hand, the height of the coal part in the combined body is lower than that of the raw single coal. Therefore, considering the scale effect, the height reduction in the coal part also leads to the enhancement of its overall bearing capacity.

Figure 6 presents the failure modes of coal and coal–rock combined bodies under uniaxial conditions. It is easy to see that under uniaxial conditions, the failure pattern of these three specimens is mainly brittle failure. Among them, the central part of the coal sample is seriously damaged, and several vertical cracks are found. Meanwhile, the coal samples are peeled off in the local area. For coal–mudstone combined body, with the increase in the loading, the microcracks firstly appear on the coal body. When approaching the peak strength, there appear many vertical cracks in the coal body. Meanwhile, some of them thread to the upper mudstone. When reaching the peak strength, the upside of the coal body is seriously broken, resulting in comminuted

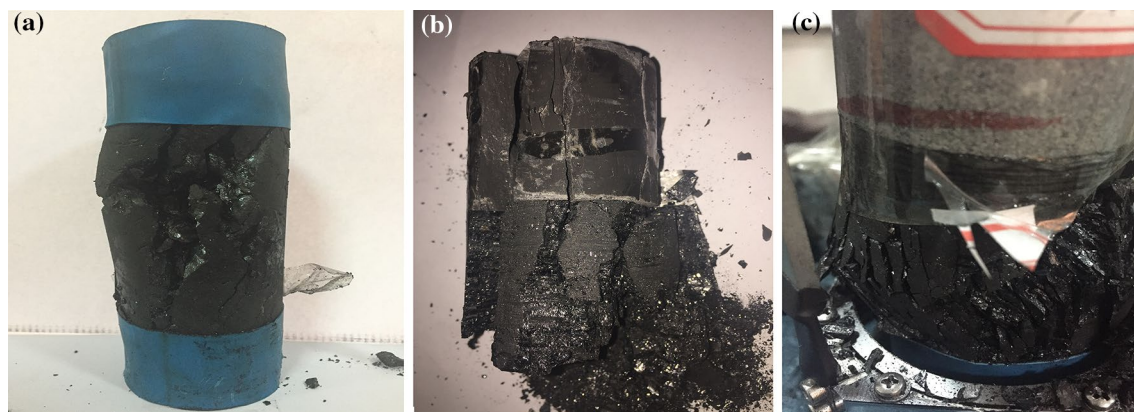


**Fig. 6** Typical failure modes of single coal and combined bodies under uniaxial conditions. **a** Coal; **b** Coal–mudstone; **c** Coal–sandstone

fracture. And a number of large cracks appear, among which two large cracks thread to the whole combined body. For coal–sandstone combined body, there are only a few vertical cracks on the side of the coal body and the cracks do not thread to the upper sandstone. This may be due to the fact that the damage strength of sandstone is much higher than that of coal, and the energy released by the failure of the coal is not enough to produce macroscopic damage.

**Deformation and failure characteristics of gas-bearing coal and coal–rock combined bodies under different confining pressures**

Table 2 presents the test results of single coals and coal–rock combined bodies under triaxial conditions. Due to the limitation of the test conditions, the measured circumferential strain is the strain of the coal body, which leads to the complexity of Poisson’s ratio and volume strain of the combined bodies. Therefore, the Poisson’s ratio and volume strain are not taken into account in the following analysis. In Table 2, *D* and *H* represent the diameter (mm) and height (mm), respectively. *E* is the elastic modulus (the slope of the stress–strain in the linear elastic phase). *V* denotes the longitudinal wave velocity and *P* is gas pressure.  $\sigma_1$ ,  $\sigma_3$  and  $\sigma_r$  are peak strength, confining pressure and residual strength, respectively. And  $\epsilon_1$ ,  $\epsilon_3$  are peak axial strain and peak circumferential strain, respectively.

**Deformation characteristics**

Typical deviatoric stress–strain curves of single coal and coal–rock combined bodies under different gas pressures and confining pressures are shown in Figs. 7, 8 and 9. For these

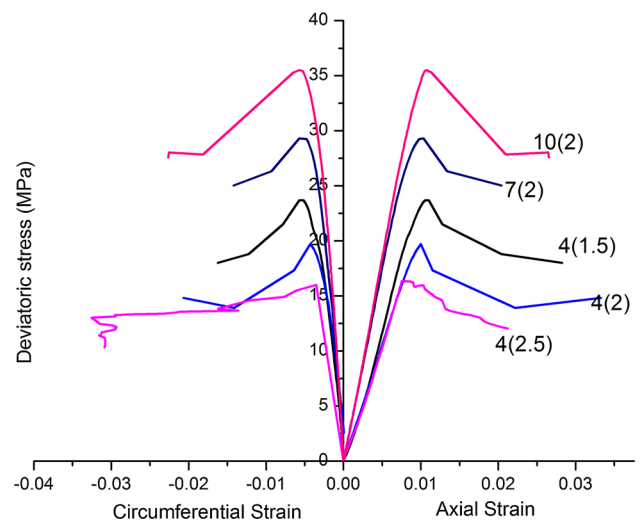


**Fig. 7** Typical deviatoric stress–strain curves of coals under triaxial conditions [“4(1.5)” represents the corresponding confining/gas pressure is 4/1.5 MPa]

three specimens, no obvious initial compression stages are shown in the stress–strain curves, and the curves mainly show present three stages: elasticity, yield and post-peak strain-softening stages. The strengths of the three specimens increase with the increase in confining pressure under consistent gas pressure, and the damage of the specimens shows obvious ductility characteristics. This is mainly because the confining pressure limits the development of deformation and crack of samples to some extent, leading to the increase in the compressive strengths of specimens. The strengths of the three specimens decrease with the increase in gas pressure under consistent confining pressure. Because the coal

**Table 2** Test results of single coal and coal–rock combined bodies under triaxial conditions

Sample	<i>D</i> (cm)	<i>H</i> (cm)	<i>V</i> (m/s)	$\sigma_3$ (MPa)	<i>P</i> (MPa)	<i>E</i> (GPa)	$\sigma_1$ (MPa)	$\sigma_r$ (MPa)	$\epsilon_1$	$\epsilon_3$
Coal	9.99	5.08	1775	4	1.5	2.757	27.69	20.81	0.011	– 0.057
	10.15	4.96	1726	4	2	2.197	23.70	17.76	0.01	– 0.0043
	10.03	4.96	1720	4	2.5	2.186	20.45	14.38	0.0078	– 0.0035
	10.10	4.96	1741	7	2	3.488	36.43	31.59	0.0103	– 0.0056
	10.04	4.98	1765	10	2	3.791	45.66	33.73	0.0107	– 0.0057
C–S	99.8	4.97	2410	4	1.5	6.333	39.1	36.01	0.0126	– 0.0142
	100.3	4.98	2395	4	2	5.921	33.63	27.90	0.0104	– 0.0131
	100.1	4.98	2363	4	2.5	5.525	29.83	21.15	0.0085	– 0.0193
	101.5	4.99	2376	7	2	4.225	44.37	30.0	0.011	– 0.0114
	100.7	5.01	2389	10	2	7.726	57.55	46.52	0.0082	– 0.0142
C–M	101.4	4.96	2648	4	1.5	7.057	37.39	20.79	0.0088	– 0.0114
	100.5	4.96	2591	4	2	4.732	25.80	20.85	0.0073	– 0.0242
	100.6	4.98	2604	4	2.5	3.483	22.48	19.74	0.0119	– 0.0097
	99.9	4.99	2689	7	2	5.516	33.05	29.11	0.0087	– 0.022
	100.8	4.96	2612	10	2	5.744	48.75	43.09	0.0132	– 0.012

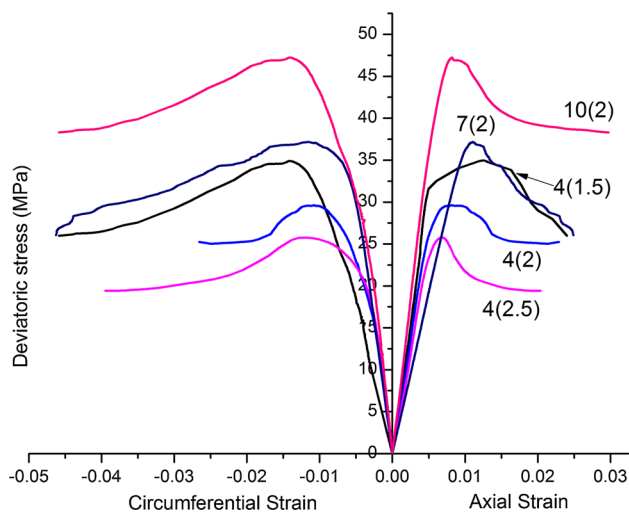


**Fig. 8** Typical deviatoric stress–strain curves of coal–sandstone combined bodies under triaxial conditions

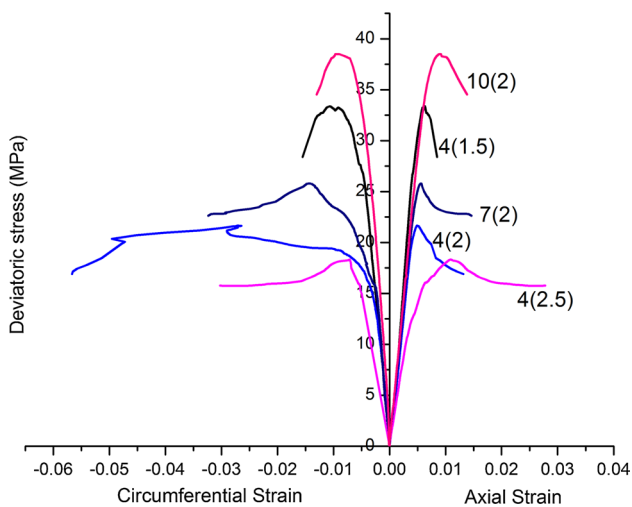


**Fig. 9** Typical deviatoric stress–strain curves of coal–mudstone combined bodies under triaxial conditions

has strong adsorbing abilities to gas and the rock basically does not adsorb gas, the strength-weakening mechanism of gas to coal and rock is not exactly the same. For coal, the influence of gas on strength is mainly mechanical and non-mechanical effect. For mechanical effect, the gas entering into the fissures of the coal in the free state not only plays important role on enlarging the volume of coal, but also provides the opposite force to the confining pressure. This force reduces the effective confining pressure of coal, which accelerates the expansion of primary cracks and the appearance of new cracks. For non-mechanical effect, the tension of micro-fracture surface decreases after adsorbing gas, which results in the decrease in the attraction between

coal molecules and reduction in the ability of matrix to bind coal molecules. Therefore, the swelling deformation of coal matrix is promoted. However, the influence of gas on rock strength is basically non-mechanical effect.

For these three specimens, with the increase in confining pressure, the peak axial strain shows an upward trend, and the absolute value of the circumferential strain shows a downward trend. With the increase in gas pressure, the peak axial strain shows a downward trend. The absolute value of the circumferential strain of the single coal sample shows a downward trend with the increase in the gas pressure, but there is no obvious relation between the circumferential strain and the gas pressure for the combined body. These may be due to two reasons. Firstly, the circumferential strain measured in this work is not the actual strain value of the combined body. Under the influence of the rock part, the circumferential strain evolution of the coal body in combined body is different from that of single coal sample. Secondly, the results may be affected by the discreteness of the specimens. Even if the wave velocities of the specimens were close, the mechanical properties might still be different. Further research is needed to fully understand the specific mechanism.

Figure 10 presents the relationship between elastic modulus and confining pressure, elastic modulus and gas pressure of different coals and coal–rock combinations. It can be seen from the figure that the change pattern of the elastic modulus is not obvious with the increase in confining pressure, which shows an increasing trend on the whole. The elastic modulus decreases with the increase in gas pressure, and the elastic modulus of single coal is smaller than that of coal–rock combined body under the same condition. Moreover, on the whole, the elastic modulus of the coal–sandstone combined body is the largest, and the elastic modulus of the single coal is the smallest.

### Failure characteristics

Typical failure modes of single coal and coal–rock combined bodies under triaxial conditions are shown in Figs. 11, 12 and 13. It can be seen from Fig. 11 that the failure characteristics of the gas-bearing coal samples are simple under the influence of confining pressure. The fracture surface is relatively unitary, and the failure mode is mainly shear failure. Moreover, the angle distribution of the cracks is related to the confining pressure and the gas pressure when the coal is damaged. With the increase in confining pressure, the failure angles of coal (the angle between the direction of fracture and the direction of maximum principal stress) are successively about 25°, 28° and 34°. Under lower confining pressure, the failure angle is lower and the fracture surface extends to the end of the coal. With the increase in confining pressure, the failure



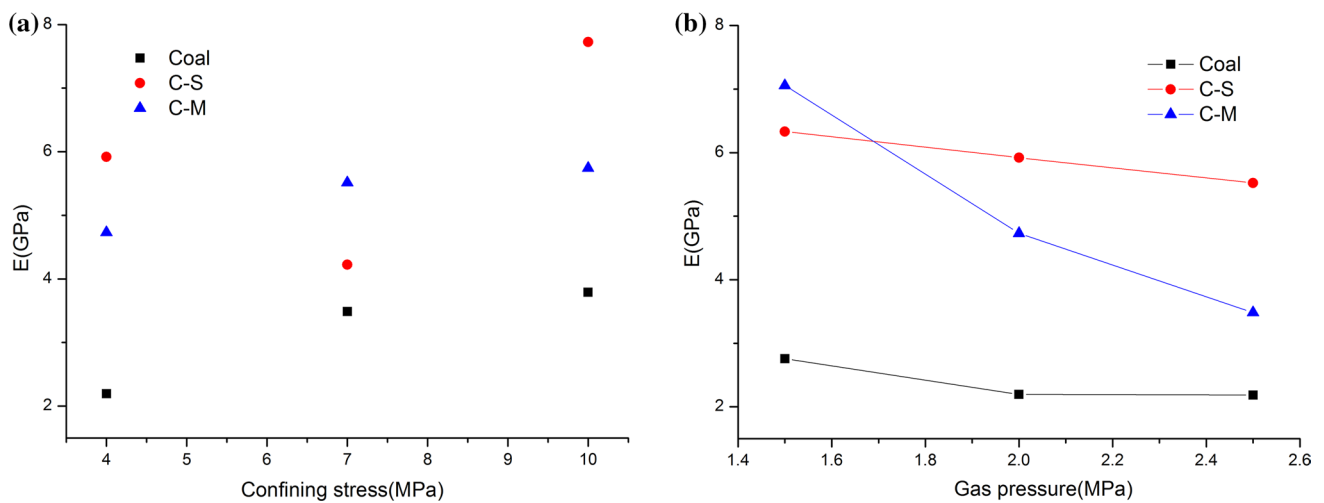


Fig. 10 The relationship between elastic modulus and confining pressure/gas pressure of different specimens

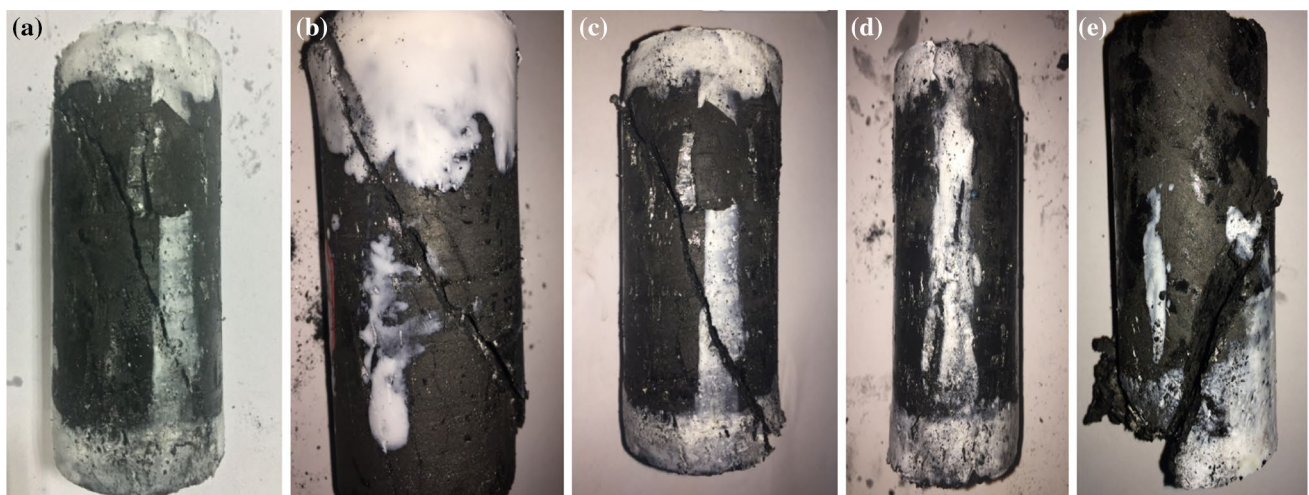
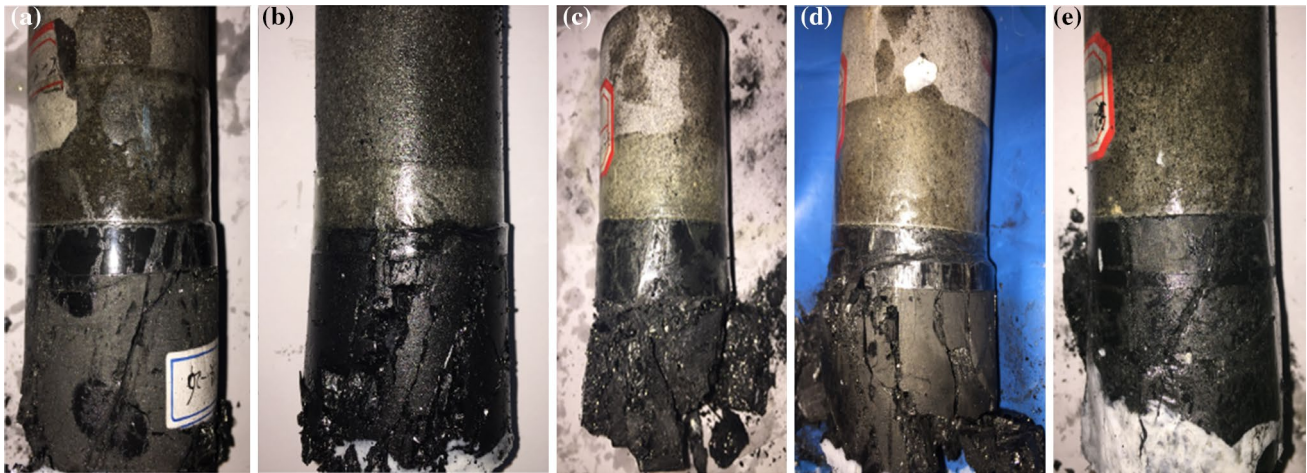


Fig. 11 Failure modes of single coals under triaxial conditions (“4–1.5” represents the corresponding confining/gas pressure is 4/1.5 MPa). a 4–1.5; b 4–2; c 4–2.5; d 7–2; e 10–2

angle becomes larger, and the fracture surface has the tendency of extending to the side. According to the Coulomb strength theory (Galindo et al. 2017), the failure angle is a fixed value, and it does not vary with the confining pressure, which is contrary to the variation law of coal sample in tests. The reason is that the envelope curve of the Coulomb strength criterion is a straight line, so the angle of internal friction obtained is unique. As a result, there is only one theoretical value of failure angle. However, in fact, according to the Mohr strength theory (Handin 1969), the internal friction angle is changeable, the Coulomb criterion is only a special case of Mohr criterion. And the Mohr strength envelope curve is external common tangent of each Mohr circles, which is not a straight line. As a result, the failure angle is a changeable value. The

influence of gas pressure on the failure mode of coal is not obvious, which needs more target research.

As can be seen from Figs. 12 and 13, the failure modes of single gas-bearing coal are different from those of coal–rock combined bodies. Coal–rock combined body is not a complete rock, but a rock with a big joint surface. Meanwhile, the strength of the rock is larger than that of the coal, and the coal body itself has a large number of joints, cracks and weak surface. And coal body will absorb a lot of gas. Therefore, in the triaxial tests, the failure of coal–rock combined bodies under different confining pressures mainly occurs in the coal bodies. However, under certain conditions, the cracks produced from the failure of the coal part will also extend to the adjacent rock part. In Fig. 12a, b, some cracks of the coal part also extend



**Fig. 12** Failure modes of coal–sandstone combined bodies under triaxial conditions. **a** 4–1.5; **b** 4–2; **c** 4–2.5; **d** 7–2; **e** 10–2

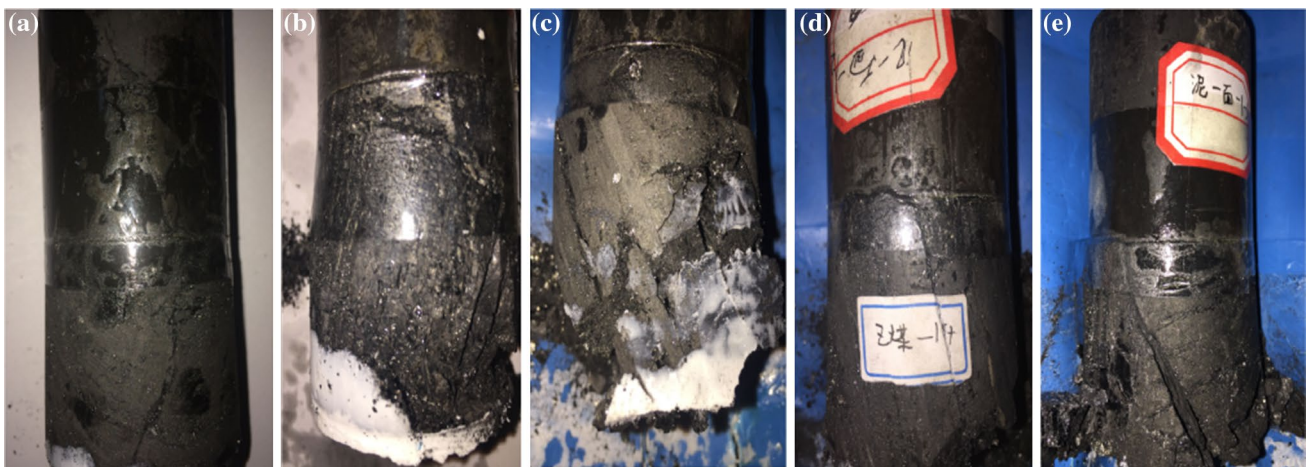


**Fig. 13** Failure modes of coal–mudstone combined bodies under triaxial conditions. **a** 4–1.5; **b** 4–2; **c** 4–2.5; **d** 7–2; **e** 10–2

to the adjacent rock part. However, the rock part did not produce macroscopic cracks in Fig. 12c–e. The reason is that under the constant confining pressure, the strength of coal decreases with the increase in gas pressure, leading to the reduction in elastic energy released by coal damage. Therefore, although the gas expansion energy becomes large, the total elastic energy and gas expansion energy released by coal damage may decrease. Moreover, the influence of gas pressure on the strength of rock is not prominent, so the energy released from the coal damage is not enough to cause the sandstone to produce macroscopic damage. Under the constant gas pressure, the elastic energy released by coal damage increases with the increment of confining pressure. Besides, the strength of sandstone also becomes greater with the increasing of confining pressure. Therefore, the energy released from the coal damage is not enough to cause the sandstone to

produce macroscopic damage. Similarly, for coal–mudstone combined body, only in Fig. 13a, d, the rock part produces macroscopic cracks.

The above results show that it is unfavorable to the damage of the rock part when the confining pressure or gas pressure is too high. Only under certain conditions, both coal part and rock part may produce macroscopic cracks for coal–rock combined body. However, it should be noted that the damage here only refers to the macroscopic damage. In most tests, it is possible to produce microscopic cracks inside the rock that are not visible to the naked eyes, which can be inferred from permeability changes in the next section. For further study of micro-cracks, some other advanced means will be needed, such as CT, transmission electron microscopy (TEM), which is the focus of our next research.

It also can be seen from Figs. 12 and 13 that the failure law of gas-bearing coal–sandstone combined body is very

similar to coal–mudstone combined body under triaxial conditions. Under constant confining pressure, with the increase in gas pressure, the surface cracks of coal part gradually change from a nearly parallel splitting crack to some parallel inclined shear cracks. For coal–sandstone combined body, with the increase in gas pressure, X-type shear cracks occur and the failure modes of coal part are changed from brittle splitting failure to ductile shear failure. For two kinds of combined bodies, under constant gas pressure, with the increase in confining pressure, the inclination angle of several parallel shear cracks becomes smaller and the number of the cracks decreases. As the confining pressure continues to increase, the coal part shows a single shear crack.

### Strength characteristics of gas-bearing coal and coal–rock combined bodies under different confining pressures

Under constant gas pressure, the peak strengths of three specimens increase with the increment of confining pressure. In order to find out the strength characteristics of gas-bearing coal and coal–rock combinations, reliable strength criterion is needed. According to the research of Zuo et al. (2016), the Mohr–Coulomb strength criterion is applicable to coal–rock combinations. Moreover, according to the research of Liu (2017), the Mohr–Coulomb strength criterion is applicable to gas-bearing coals. However, whether the criterion is applicable to gas-bearing coal–rock combinations is rarely mentioned. In this section, the Coulomb strength criterion is used to fit the triaxial compression test data of gas-bearing coals and coal–rock combined bodies under different confining pressures. The fitting results are shown in Fig. 14. Under the 2 MPa of gas pressure, the strengths of the pure coal and coal–sandstone combined bodies show a linear relationship with the confining pressure,

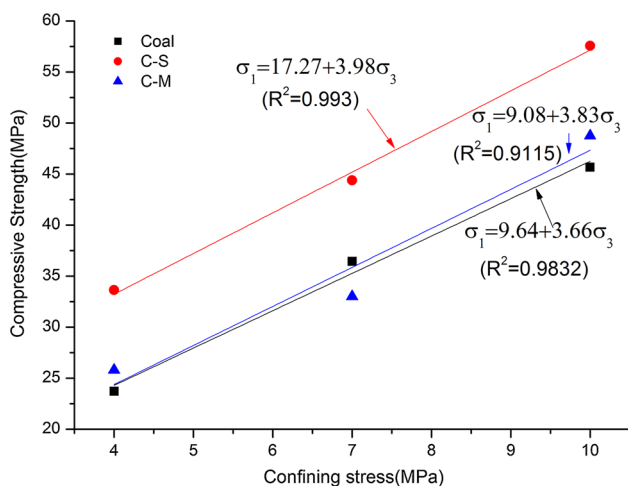


Fig. 14 Fitting curves of Mohr–Coulomb strength criterion

and the R-square is about 99%. For coal–mudstone combined body, the strength basically shows a linear relationship with the confining pressure, the R-square is 91%. The reason for this result may be that the number of tests is relatively small, and the discreteness of the coal sample itself is very large. Therefore, the test results are inevitably accidental. However, in general, the Coulomb strength criterion is applicable to gas-bearing coal–rock combined body. According to the research of Zuo et al. (2016), the Hoek–Brown strength criterion and generalized Hoek–Brown strength criterion are all applicable to coal–rock combined body. However, due to the limitation of experimental conditions, the uniaxial strengths of all samples under 2 MPa of gas pressure have not been measured. Therefore, in this work, it is impossible to verify whether the Hoek–Brown strength criterion and the generalized Hoek–Brown strength criterion are applicable to gas-bearing coal–rock combined bodies, which will be the focus of our future research.

Figure 15 presents the relationships between confining pressure and residual strength, gas pressure and residual strength and gas pressure and peak strength. With the increase in gas pressure, the peak strength and residual strength of coal sample decrease gradually. With the increase in confining pressure, the residual strength of coal sample increases gradually.

### Permeability evolution of gas-bearing coals and coal–rock combined bodies under different confining pressures

While coal–gas compound dynamic disasters occur, a large amount of gas in rock of roof (floor) and the nearby coal seam may flow into the working face and flush into the disaster site, which results in more serious damages. Therefore, it is important for further understanding of the mechanism of coal–gas compound dynamic disasters to study the gas flow behavior in the coal–rock combined bodies. Especially, it is of great significance to study the seepage characteristics during the process of the disasters.

Assuming that gas permeation through the sample is an isothermal process, and the coal or rock body can be regarded as isotropic homogeneous material, the gas permeability can be calculated from Darcy’s law (Somerton et al. 1975):

$$k = \frac{2\mu P_a L Q}{A(P_1^2 - P_2^2)} \tag{1}$$

where  $k$  denotes permeability (mD),  $Q$  denotes gas flow rate ( $\text{cm}^3/\text{s}$ ),  $P_a$  denotes atmospheric pressure (0.1 MPa),  $A$  denotes cross-sectional area of the sample ( $\text{cm}^2$ ),  $L$  denotes sample length (mm),  $P_1$  denotes inlet gas pressure (MPa),

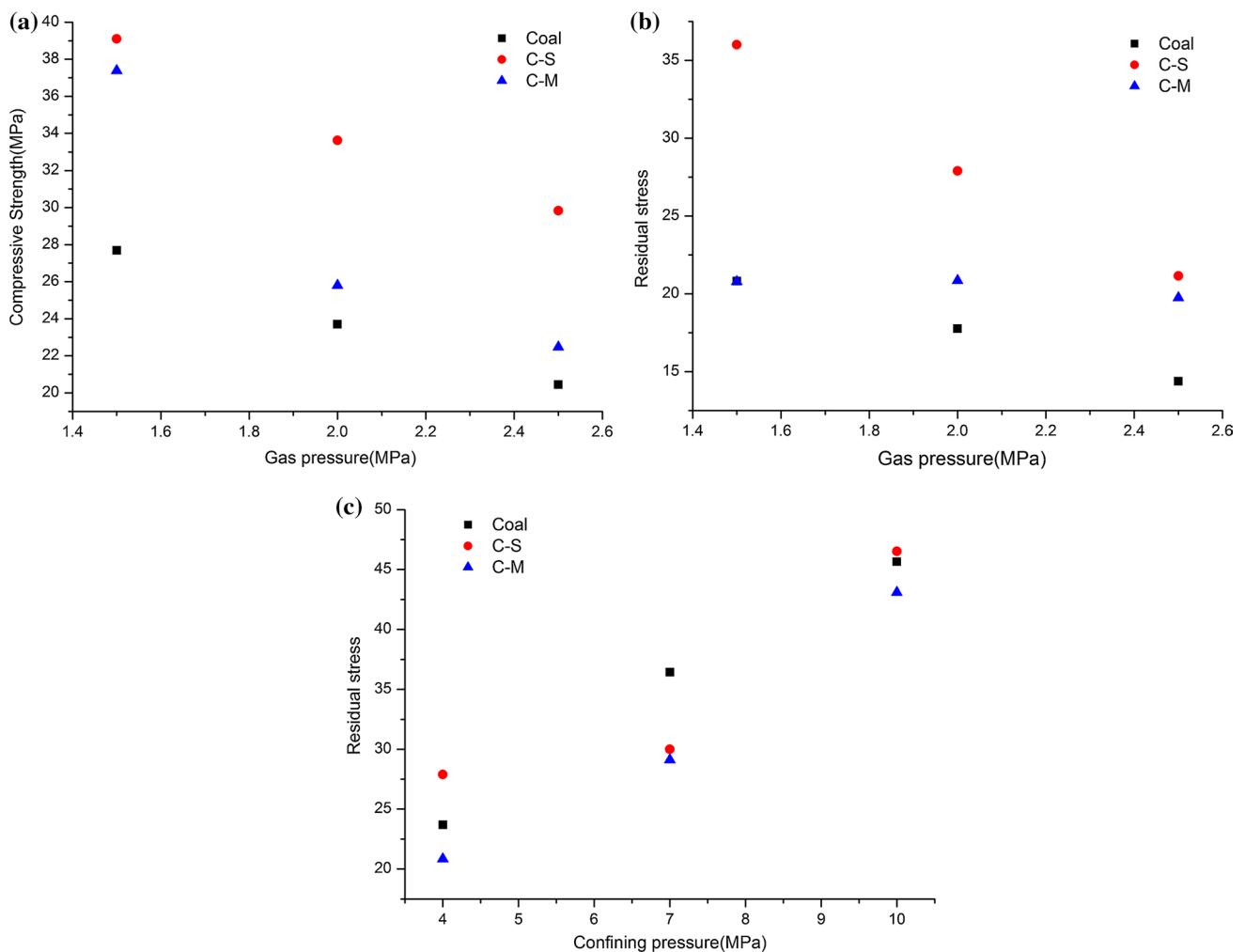


**Fig. 15** The relationships between specific parameters. **a** Gas pressure and peak strength; **b** Gas pressure and residual strength; **c** Confining pressure and residual strength

$P_2$  denotes outlet gas pressure (MPa) and  $\mu$  denotes gas viscosity (MPa s).

It should be noted that, according to Darcy's law and the research of Amyx et al. (1960) on average permeability of the series combination of beds, the average permeability can still be evaluated in Darcy's law (Fig. 16). It is assumed that two coal seams with different permeabilities ( $K_1$ ,  $K_2$ ) are superimposed together, and thickness of the seams is  $L_1$  and  $L_2$ , respectively, then the average permeability of combined body can be evaluated as follows:

$$k = \frac{L_1 + L_2}{\frac{L_1}{K_1} + \frac{L_2}{K_2}} = \frac{\sum_{i=1}^n L_i}{\sum_{i=1}^n \frac{L_i}{K_i}} \quad (2)$$

It can be inferred from above formula, since the permeability of sandstone and mudstone is much smaller than that of coal, the permeability of the coal-rock combined body

is basically determined by the rock part before the failure of the combined body. Figures 17, 18 and 19 present axial stress-strain curves and axial strain-permeability curves under triaxial tests.

As shown in Fig. 17, for single coal sample, with the increase in axial deviatoric stress, the changes of gas permeability show a tendency of an initial decrease, and subsequent increase. In the compaction and elastic deformation stage of coals, the primary fracture and pore of coals are closed gradually. Therefore, the permeability decreases with the rise of axial deviatoric stress. As the axial loading continues to increase, the initiation and propagation of cracks in coals provide new channels for gas flow. As a result, the permeability shows a trend of slow increase. As the axial deviatoric stress continues to increase, the expansion rate of primary and new fractures is accelerated. Then, at the peak point of sample, the cracks are connected with each other, leading to the macroscopic fractures of coals. The

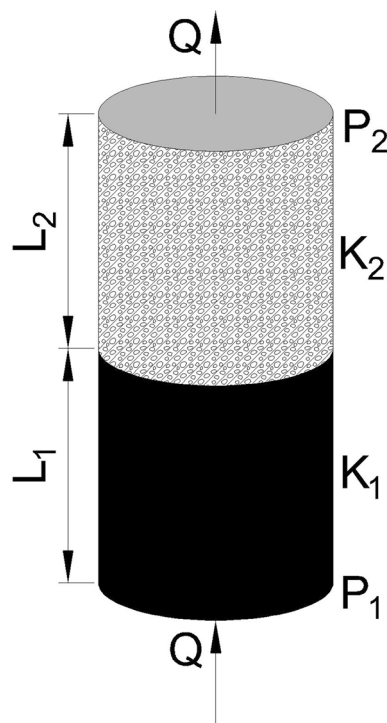


**Fig. 16** Schematic diagram of linear seepage in coal–rock combined body

broken coal pieces were dislocated along the fracture surface, increasing the normal spacing of macro-fractures. In the stress drop stage, a fully penetrating network is formed. Therefore, the permeability increases rapidly and exceeds the initial permeability. Under the condition of a 10-MPa confining stress and a 2-MPa gas pressure, the permeability does not exceed the initial permeability. It is probably because that the macroscopic fracture of coal only occurs in a region on the side of the coal, and the large crack does not penetrate the coal body. While the sample comes into residual stage, the strength of coal is provided by the shearing stress between the fracture surfaces, and the severe structure motion stops. If the shear slip and propagation of cracks cause the coal sample to continue to form a macroscopic fracture, the permeability continues to increase. But the increase rate is lower than that of post-peak failure stage. If the sample does not continue to generate macroscopic cracks, the seepage channel becomes relatively stable and the permeability will have minor increase and even becomes stable.

It can be seen from Figs. 18 and 19, for coal–rock combined bodies, the changes of gas permeability show a similar trend with coals in the compaction and elastic deformation stage. In post-peak failure stage, the penetrating cracks in the coal body are basically formed in all combined bodies. As these cracks penetrate into the upper portion of the rock part and a fully penetrating network is formed, the permeability

increases rapidly and exceeds the initial permeability. The coal–sandstone combined bodies (4–1.5, 4–2) and coal mudstone combined body (4–1.5, 4–2, 7–2) exhibit such property. From the view of the photograph, only coal–sandstone combined body at a confining pressure of 4 MPa and gas pressure of 2 MPa (4–2) has a very significant penetrating crack. The remaining four surfaces of specimens do not generate such crack. It can be inferred from permeability curves of these four specimens that huge damages have occurred inside the rock part of the samples so that permeability has increased dramatically. When coal cracks in the combined body penetrate to the upper portion of the rock part but a fully penetrating network has not formed, the permeability increases but still lower than the initial permeability. Coal (10, 2), coal–sandstone combined body (4–2.5, 7–2) and coal–mudstone combined body (4–2) prove said process. In these cases, the permeability at the residual stage does not increase substantially. At a confining pressure of 10 MPa and gas pressure of 2 MPa, the permeabilities of two kinds of combined bodies have dropped to almost 0 mD during the elastic stage and the permeabilities are still close to 0 mD at post-peak stage and residual stage. The reason is that the some fractures and pores of the coal part and rock part are compressed as a result of high confining pressure, which leads to very low initial permeability before triaxial loading. With the increase in axial deviatoric stress, the fractures and pores are further compressed and then the permeability drops to 0 mD. When the coal sample is damaged, due to the great strength of the rock part, no macroscopic cracks and obvious internal damage occur. Therefore, the permeability is still near 0 mD.

Thus, the permeability evolution of gas-bearing coal and coal–rock combination bodies during the failure process is not exactly the same and is closely related to the crack propagation in the coals and rocks. The crack propagation not only determines the macroscopic stress–strain characteristics of the coals and coal–rock combination bodies, but also determines its permeability evolution. In this paper, it is only a preliminary study on the seepage characteristics of coal–rock combination bodies during deformation and failure process. To thoroughly understand the underlying mechanism, further targeted researches are required.

## Discussion

From the results of this work, it is obtained that when other conditions are held constant, the strength relationship between gas-bearing coal and coal–rock combined bodies is: coal–sandstone combined body > coal–mudstone combined body > coal. Gas also has a great influence on the mechanical properties of coal–rock combined bodies. Therefore, in order to find out the mechanism of coal–gas compound

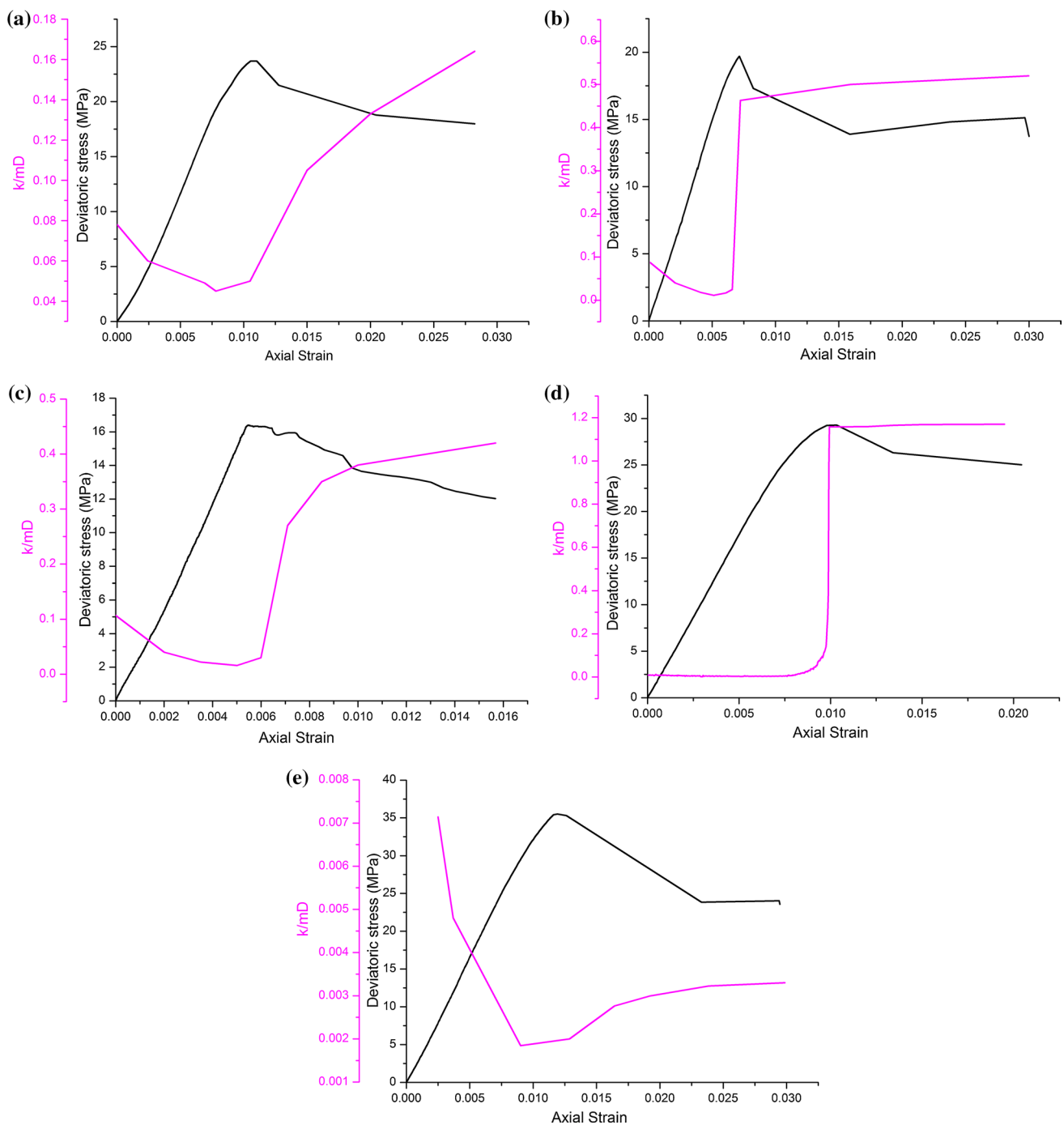


**Fig. 17** Stress–strain curves and axial strain–permeability curves of coals under triaxial tests. **a** 4–1.5; **b** 4–2; **c** 4–2.5; **d** 7–2; **e** 10–2

dynamic disaster, we should conduct researches combing the gas, coal and rock as a whole system. Under different stress and gas conditions, the failure forms between different combinations (coal–mudstone, coal–sandstone) under the action of external force caused by mining disturbance have relatively big difference. Therefore, the types and characteristics of dynamic disasters are not the same. For coal–rock combined body, since the softening effect of gas on coal is

greater than that on rock, the strength of combined body is determined by gas-bearing coal part. When the confining pressure is constant (such as 4 MPa in this work), with the increase in the gas pressure, the strength of the combined body becomes smaller, and the strength difference between rock part and coal part becomes larger. For coal–sandstone combined body under low gas pressure (such as 1.5 MPa), when the combined body is damaged, the elastic energy

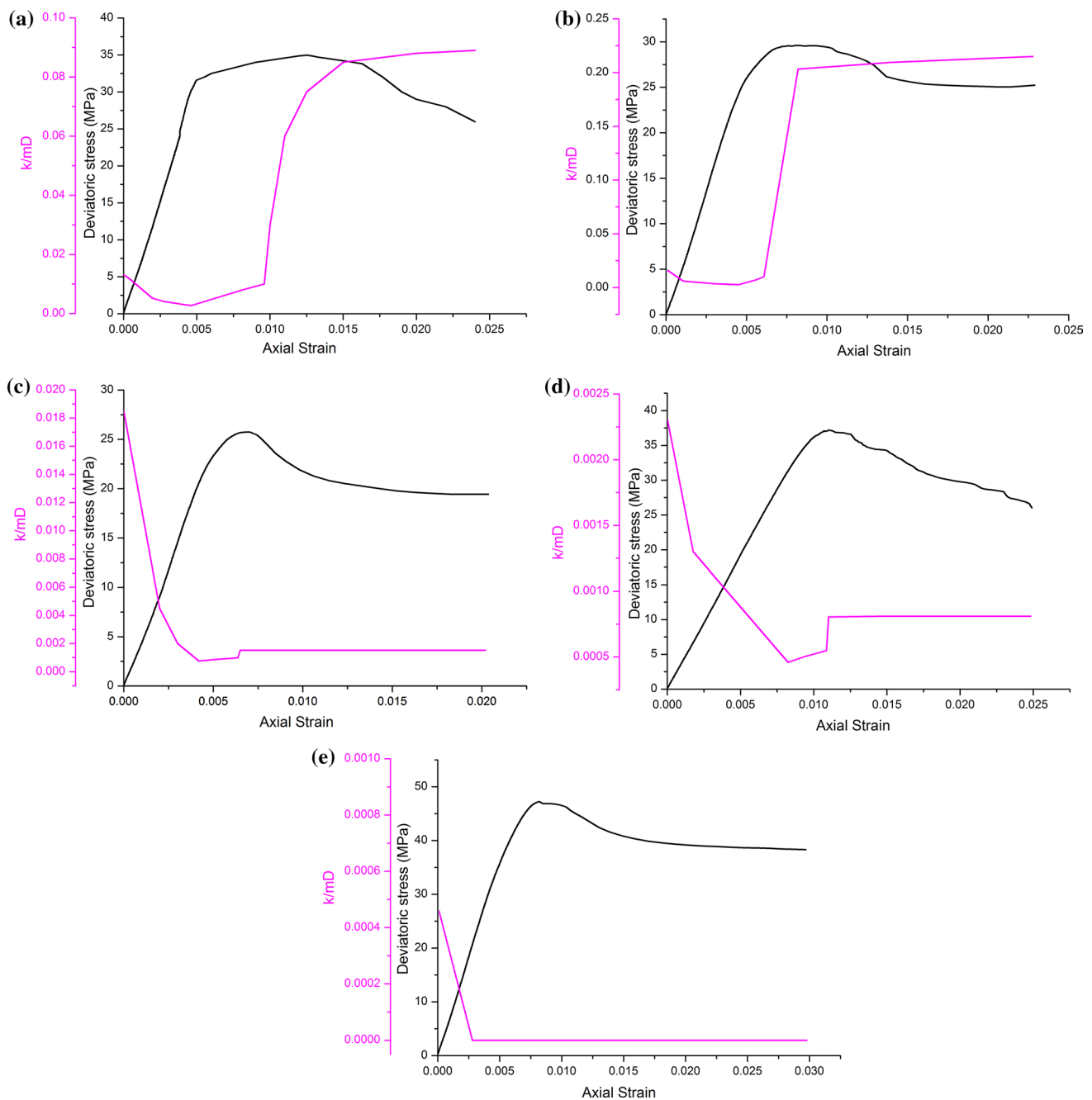


**Fig. 18** Stress–strain curves and axial strain–permeability curves of coal–sandstone combined bodies under triaxial tests. **a** 4–1.5; **b** 4–2; **c** 4–2.5; **d** 7–2; **e** 10–2

released by coal and rock may be much larger than the gas expansion energy, and the corresponding disaster type is mainly rockburst. With the increase in gas pressure (such as 2 MPa), the strength of coal and rock becomes lower and the combined body is relatively easy to damage. When the combined body is damaged, the elastic energy released by coal and rock is lower than that under low gas pressure. Meanwhile, because the gas at relatively high pressure will release some gas expansion energy, the combined body

would be damaged under the combined action of coal and rock elastic energy and gas expansion energy. And the corresponding disaster type is mainly outburst and rockburst coupling dynamic disaster. With the continuous increase in gas pressure (2.5 MPa), the strength difference between rock part and coal part becomes larger. Because of higher gas pressure, the damage of combined body is only the damage of coal part in a relatively short time, and the larger gas expansion energy is released. However, the released

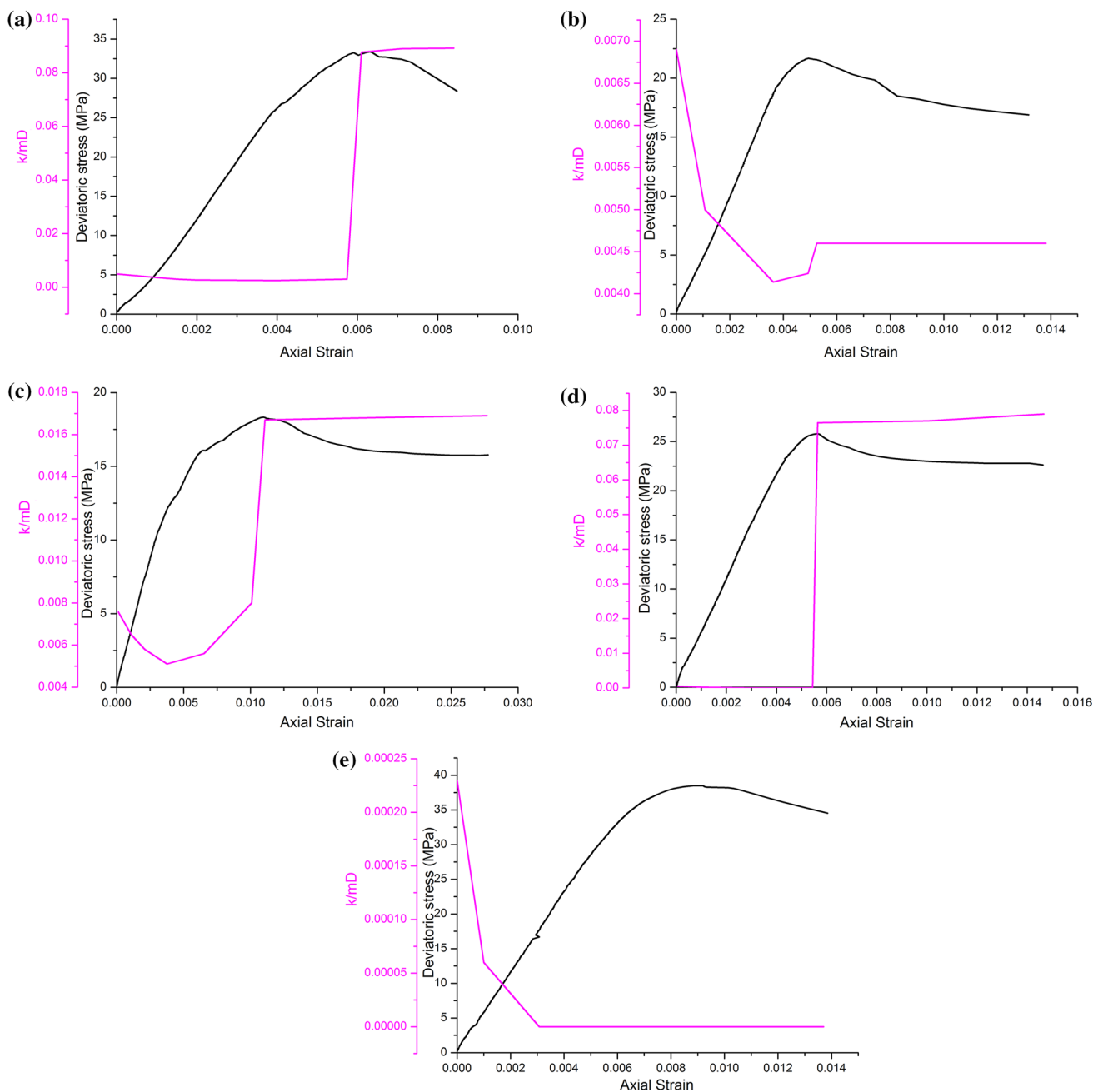


**Fig. 19** Stress–strain curves and axial strain–permeability curves of coal–mudstone combined bodies under triaxial tests. **a** 4–1.5; **b** 4–2; **c** 4–2.5; **d** 7–2; **e** 10–2

elastic energy of coal and rock is relatively small, and the corresponding disaster type is mainly coal and gas outburst. When the gas pressure is constant, with the increase in the confining pressure, the strength of the combined body becomes larger, and the strength difference between rock part and coal part also becomes larger. Therefore, the damage of combined body is mainly the damage of coal part, and the disaster type is transitioning to rockburst. The failures of coal–mudstone combined body and coal–sandstone

combined body show similar pattern. The difference is that the strength of mudstone is lower than that of sandstone in combined body. Therefore, when the coal–gas compound dynamic disaster occurs, the gas pressure in the coal–mudstone combined body is relatively smaller (e.g., 1.5 MPa) or confining pressure is relatively greater (e.g., 7 MPa) than those in coal–sandstone combined body.

When the coal–gas compound dynamic disaster occurs, the permeability of coal–rock combined body will increase



dramatically, see coal–sandstone combined body (4–2), coal–mudstone combined body (4–1.5, 7–2). It creates favorable conditions for a large amount of gas flowing out from adjacent coal seams and roof (floor), which makes the damage more serious and brings great loss of life and property. When the disaster type is only rockburst, the permeability of coal–rock combined body will also increase dramatically. However, due to the low content of gas stored in the coal and rock, the occurrence of rockburst is not accompanied by serious gas disaster in most cases. When the disaster type is only coal and gas outburst, the permeability of coal–rock combined body will not increase dramatically in most cases, and it is difficult for a large amount of gas flowing out from adjacent coal seams and roof (floor).

It is shown in present work that the occurrence of coal–gas compound dynamic disaster is the result of coupling effect of stress field, fracture field and seepage field. This work is only a preliminary study. In the future, more fundamental researches should be conducted taking coal, rock and gas as a whole system. The fracture behavior and gas seepage characteristics in the process of coal–gas compound dynamic disasters should be further investigated. It is also of great significance to study the interaction mechanism of coal, rock and gas in the process of compound dynamic disaster and provide a scientific basis for the prevention and control of coal–gas compound dynamic disasters.

## Conclusions

- (1) Under uniaxial conditions, the brittle failures are the main failure modes for all of the specimens. The stress–strain curves of the five specimens have undergone five stages: fracture compression, elastic deformation, plastic deformation, strain softening and plastic flow. After the peak stress, the stress shows obvious “stress drop” phenomenon, and the dropping velocities of different specimens are different: sandstone > mudstone > coal–sandstone combined body > coal–mudstone combined body > coal.
- (2) Under triaxial conditions, the strengths of all specimens increase and ductile failure characteristics are much more apparent with the increment of confining pressure or with the decrease in the gas pressure and the elastic modulus shows a tendency of increase in general. The strength of the coal–rock combination body falls in between the single rock and coal, and the strength of coal–sandstone combined body is larger than that of coal–mudstone combined body.
- (3) The failure characteristics of the gas-bearing coal samples are simple under the influence of confining pressure. The fracture surface is relatively unitary,

and the failure mode is mainly shear failure. However, the failure modes of coal–rock combined bodies are different from those of single gas-bearing coals. And the failure of coal–rock combined body mainly occurs in the coal body. However, under certain conditions, the cracks produced from the failure of the coal part will also extend to the adjacent rock part. The strength characteristics of gas-bearing coals and coal–rock combination bodies all met Mohr–Coulomb criterion, and the residual strength has an increasing trend with the increase in confining pressure or with the decrease in the gas pressure.

- (4) The permeability evolutions of gas-bearing coal and coal–rock combination bodies are not exactly the same, which are determined by the crack propagation in the coal and rock.

**Acknowledgements** The authors gratefully appreciate Mr. Siyi Guo for his assistance on the final language editing on this paper. The authors acknowledge the support of the State Key Research Development Program of China (2016YFC0600708, 2016YFC0801402), the National Natural Science Foundation of China (51474219, 51604153, 51604278), the Joint Fund Project of Guizhou Science and Technology Department and Bijie Science and Technology Bureau and Institute of Circular Economy (LH[2014]7520) and the Guizhou Science and Technology Support Program ([2017]2820). The authors also thank two anonymous reviewers for valuable suggestions that helped improve the manuscript.

## Compliance with ethical standards

**Conflict of interest** All the authors declare that they have no conflict of interest.

## References

- Amyx J, Bass D, Whiting R (1960) Petroleum reservoir engineering. McGraw-Hill, New York
- Bao CY, Tang CA, Cai M, Tang SB (2013) Spacing and failure mechanism of edge fracture in two-layered materials. *Int J Fract* 181:241–255
- Busch A, Gensterblum Y (2011) CBM and CO<sub>2</sub>-ECBM related sorption processes in coal: a review. *Int J Coal Geol* 87:49–71
- Chen G (2013) Analysis of coal and gas outburst induced rock burst accidents in Yangou Coal Mine. *Saf Coal Min* 44:156–158 (in Chinese)
- Chen ZH, Fu YF, Tang CA (1997) Experimental study of interaction of two rock specimen under uniaxial compression. *J Northeast Univ* 18:382–385 (in Chinese)
- Clarkson CR, Bustin RM (1999) The effect of pore structure and gas pressure upon the transport properties of coal: a laboratory and modeling study. 1. Isotherms and pore volume distributions. *Fuel* 78:1333–1344
- Day S, Fry R, Sakurovs R (2012) Swelling of coal in carbon dioxide, methane and their mixtures. *Int J Coal Geol* 93:40–48
- Deng XB, Hu HJ, Xu G, Li XT, Chen FY (2012) Numerical simulation for burst failure of two-body rock structure. *J Min Saf Eng* 29:833–839 (in Chinese)

- Dou LM, Tian JC, Lu CP et al (2005) Research on electromagnetic radiation rules of composed coal–rock burst failure. *Chin J Rock Mech Eng* 24:3541–3544 (in Chinese)
- Galindo RA, Serrano C, Olalla C (2017) Ultimate bearing capacity of rock masses based on modified Mohr–Coulomb strength criterion. *Int J Rock Mech Min Sci* 93:215–225
- Gensterblum Y, Merkel A, Busch A, Krooss BM (2013) High-pressure CH<sub>4</sub> and CO<sub>2</sub> sorption isotherms as a function of coal maturity and the influence of moisture. *Int J Coal Geol* 118:45–57
- George JDS, Barakat MA (2001) The change in effective stress associated with shrinkage from gas desorption in coal. *Int J Coal Geol* 45:105–113
- Guo DM, Zuo JP, Zhang Y et al (2011) Research on strength and failure mechanism of deep coal–rock combination bodies of different inclined angles. *Rock Soil Mech* 5:1333–1339 (in Chinese)
- Handin J (1969) On the Coulomb–Mohr failure criterion. *J Geophys Res* 74:5343–5348
- Huang BX, Liu JW (2013) The effect of loading rate on the behavior of samples composed of coal and rock. *Int J Rock Mech Min Sci* 61:23–30
- Iannacchione AT, Zelanko JC (1995) Occurrence and remediation of coal mine bumps: a historical review. Paper presented at the Proceedings of mechanics and mitigation of violent failure in coal and hard-rock mines. US Bureau of Mines Special Publication
- Lama RD, Bodziony J (1998) Management of outburst in underground coal mines. *Int J Coal Geol* 35:83–115
- Li T, Cai MF, Cai M (2007) A review of mining-induced seismicity in China. *Int J Rock Mech Min Sci* 44:1149–1171
- Li LC, Tang CA, Wang SY (2012) A numerical investigation of fracture infilling and spacing in layered rocks subjected to hydro-mechanical loading. *Rock Mech Rock Eng* 45:753–765
- Li ZH, Wang EY, Ou JC, Liu ZT (2015) Hazard evaluation of coal and gas outbursts in a coal–mine roadway based on logistic regression model. *Int J Rock Mech Min Sci* 80:185–195
- Lin P, Tang CA, Chen ZH (1999) Numerical and experimental study of deformation and failure behavior in a double rock specimen system. *Earthquake* 19:413–418 (in Chinese)
- Liu KD (2017) Mechanical properties of ram coal containing gas under high triaxial stress compression. *Chin J Rock Mech Eng* 36:380–393 (in Chinese)
- Liu B, Yang RS, Guo DM (2004a) Burst-prone experiments of coal–rock combination at 1100 m level in Suncun coal mine. *Chin J Rock Mech Eng* 23:2402–2408 (in Chinese)
- Liu JH, Tang CA, Zhu WC (2004b) Rock–coal model for studying the rockburst. *Chin J Geotech Eng* 26:275–280 (in Chinese)
- Liu J, Wang EY, Song DZ et al (2014) Effect of rock strength on failure mode and mechanical behavior of composite samples. *Arab J Geosci* 8:1–13
- Masoudian MS, Airey DW, El-Zein A (2014) Experimental investigations on the effect of CO<sub>2</sub> on mechanics of coal. *Int J Coal Geol* 128–129:12–23
- Palmer I, Mansoori J (1996) How permeability depends on stress and pore pressure in coalbeds: a new model. *SPE Reserv Eval Eng* 1:539–544
- Pan YS (2016) Integrated study on compound dynamic disaster of coal–gas outburst and rockburst. *J China Coal Soc* 41:105–112 (in Chinese)
- Perera MSA, Ranjith PG, Viete DR (2013) Effects of gaseous and super-critical carbon dioxide saturation on the mechanical properties of bituminous coal from the Southern Sydney Basin. *Appl Energy* 110:73–81
- Petukhov IM, Linkov A (1979) The theory of post-failure deformations and the problem of stability in rock mechanics. *Int J Rock Mech Min Sci* 16:57–76
- Ranjith PG, Jasinge D, Choi SK, Mehic M, Shannon B (2010) The effect of CO<sub>2</sub> saturation on mechanical properties of Australian black coal using acoustic emission. *Fuel* 89:2110–2117
- Siriwardane H, Haljasmaa I, McLendon R, Irdi G, Soong Y, Bromhal G (2009) Influence of carbon dioxide on coal permeability determined by pressure transient methods. *Int J Coal Geol* 77:109–118
- Somerton WH, Söylemezoğlu IM, Dudley RC (1975) Effect of stress on permeability of coal. *Int J Rock Mech Min Sci* 12:129–145
- Sun XH, Li T (2011) prevention theory and technology on compound dynamic disaster of deep mining in coal mine. Science Press, Beijing (in Chinese)
- Tan YL, Guo WY, Gu QH et al (2016) Research on the rockburst tendency and AE characteristics of inhomogeneous coal–rock combination bodies. *Shock Vib* 2016:1–11
- Viete DR, Ranjith PG (2007) The mechanical behaviour of coal with respect to CO<sub>2</sub> sequestration in deep coal seams. *Fuel* 86:2667–2671
- Wang XB (2006) Numerical simulation of deformation and failure for bodies model composed of rock and coal. *Rock Soil Mech* 27:1066–1070 (in Chinese)
- Wang XN, Lu CP, Xue JH et al (2013) Experimental research on rules of acoustic emission and microseismic effects of burst failure of compound coal–rock samples. *Rock Soil Mech* 34:2569–3575 (in Chinese)
- Wang K, Du F, Wang G (2017a) Investigation of gas pressure and temperature effects on the permeability and steady-state time of Chinese anthracite coal: an experimental study. *J Nat Gas Sci Eng* 40:179–188
- Wang K, Du F, Wang G (2017b) The influence of methane and CO<sub>2</sub> adsorption on the functional groups of coals: insights from a Fourier transform infrared investigation. *J Nat Gas Sci Eng* 45:358–367
- Xie J, Gao MZ, Yu B, Zhang R, Jin WC (2015) Coal permeability model on the effect of gas extraction within effective influence zone. *Geomech Geophys Geo Energy Geo Resour* 1:15–27
- Yang SQ, Xu P, Xu T (2015) Nonlinear visco-elastic and accelerating creep model for coal under conventional triaxial compression. *Geomech Geophys Geo Energy Geo Resour* 1:109–120
- Zhang ZT, Liu JF, Wang L et al (2012) Effects of combination mode on mechanical properties and failure characteristics of the coal–rock combinations. *J China Coal Soc* 10:1677–1681 (in Chinese)
- Zhao YX, Jiang YD, Zhu J et al (2008) Experimental study on precursory information of deformations of coal–rock composite samples before failure. *Chin J Rock Mech Eng* 27:339–346 (in Chinese)
- Zhao SK, Zhang Y, Han RJ, Jiang HB, Zhang NB (2013a) Numerical simulation experiments on bursting liability evolution of compound coal–rock structure. *J Liaoning Tech Univ (Nat Sci)* 32:1441–1446 (in Chinese)
- Zhao ZH, Wang WM, Yan JX (2013b) Strain localization and failure evolution analysis of soft rock–coal–soft rock combination model. *J Appl Sci* 13:1094–1099
- Zhao ZH, Wang WM, Dai CQ, Yan JX (2014) Failure characteristics of three-body model composed of rock and coal with different strength and stiffness. *Trans Nonferrous Metal Soc China* 24:1538–1546
- Zhao ZH, Wang WM, Wang LH, Dai CQ (2015) Compression-shear strength criterion of coal–rock combination model considering interface effect. *Tunn Undergr Space Technol* 25:456–468
- Zhao ZH, Lv XZ, Wang WM, Tan YL (2016) Damage evolution of bi-body model composed of weakly cemented soft rock and coal considering different interface effect. *Springer Plus* 25:456–468
- Zhu GA, Dou LM, Cai W, Li ZL, Zhang M, Kong Y, Shen W (2016a) Case study of passive seismic velocity tomography in rock burst hazard assessment during underground coal entry excavation. *Rock Mech Rock Eng* 49:1–11

- Zhu ZH, Feng T, Gong FQ et al (2016b) Experimental research of mechanical properties on grading cycle loading-unloading behavior of coal-rock combination bodies at different stress levels. *J Cent South Univ (Sci Technol)* 47:2469–2475 **(in Chinese)**
- Zuo JP, Pei JL, Liu JF et al (2011a) Investigation on acoustic emission behavior and its time-space evolution mechanism in failure process of coal-rock combined body. *Chin J Rock Mech Eng* 30:1564–1570 **(in Chinese)**
- Zuo JP, Xie HP, Meng BB et al (2011b) Experimental research on loading-unloading behavior of coal-rock combination bodies at different stress levels. *Rock Soil Mech.* 5:1287–1296 **(in Chinese)**
- Zuo JP, Chen Y, Zhang JW et al (2016) Failure behavior and strength characteristics of coal-rock combined body under different confining pressures. *J China Coal Soc* 41:2706–2713 **(in Chinese)**